Available online at www.sciencedirect.com
SCIENCE DIRECT®
International Journal of Heat and Mass Transfer 47 (2004) 3171–3186
International Journal of HEAT and MASS TRANSFER
www.elsevier.com/locate/ijhmt

The effects of topology upon fluid-flow and heat-transfer within cellular copper structures

J. Tian [a], T. Kim [a], T.J. Lu [a,*], H.P. Hodson [a], D.T. Queheillalt [b], D.J. Sypeck [c], H.N.G. Wadley [b]

[a] Department of Engineering, University of Cambridge, Trumpington Street, Cambridge CB2 1PZ, UK
[b] Materials Science Department, School of Engineering and Applied Sciences, University of Virginia, Charlottesville, VA 22903, USA
[c] Aerospace Engineering Department, Embry-Riddle Aeronautical University, 600 S. Clyde Morris Blvd., Daytona Beach, FL 32114, USA

Received 19 September 2002; received in revised form 12 February 2004
Available online 20 March 2004

Abstract

The fluid-flow and heat-transfer features of cellular metal lattice structures made from copper by transient liquid phase (TLP) bonding and brazing of plane weave copper meshes (screens) were experimentally characterized under steady-state forced air convection. Due to the inherent structural anisotropy of this metal textile derived structure, the characterizations were performed for several configurations to identify the preferable orientation for maximizing thermal performance as a heat dissipation medium. Results show that the friction factor of bonded wire screens is not simply a function of porosity as stochastic materials such as open-celled metal foams and packed beds, but also a function of orientation (open area ratio). The overall heat transfer depends on porosity and surface area density, but only weakly on orientation. Comparisons with stochastic metal foams and other heat dissipation media such as packed beds, louvered fins and microtruss lattice cellular materials suggest that wire-screen meshes compete favorably with the best available heat dissipation media. The overall thermal efficiency index of the copper textiles-based media is approximately three times larger than that of stochastic copper foams, principally because of the lower pressure drop encountered during coolant propagation through the periodic wire-screen structure.

Keywords: Forced convection; Cellular metals; Woven textiles; Louvered fins; Packed beds; Experiment; Thermal efficiency

1. Introduction

High porosity, ultra-lightweight, cellular metal structures with open cell topologies have emerged in the past decade as attractive heat exchange media for a wide range of applications where dissipation of high intensity heat over relatively small spaces is demanded [1,2]. These cellular metal structures can be classified into two broad classes, one with a stochastic topology (i.e. metal foams) and the other with a periodic structure [3–7]. A schematic illustration of several open and one close celled periodic structure is shown in Fig. 1. Examples of the periodic structure include materials made from stacked metal textiles and microtruss concepts with tetrahedral, pyramidal, Kagome and other types of topologies [3,4]. A wide variety of process-routes have been developed to manufacture cellular metals with relative densities of 1–20% and cell sizes from 100 μm to several centimetres [5]. The open cell systems shown in Fig. 1(a)–(e) compare favourably with closed cell honeycombs (Fig. 1f) when used for the cores of sandwich panels [7]. They are therefore attracting considerable attention as multi-functional structures [7].

Several mechanisms contribute to heat transfer enhancements associated with the use of cellular metals, including interactions between the solid skeleton and a through-flowing fluid, and the importance of achieving a

* Corresponding author. Tel.: +44-1223-766316; fax: +44-1223-332662.
E-mail address: tjl21@cam.ac.uk (T.J. Lu).

0017-9310/$ - see front matter © 2004 Elsevier Ltd. All rights reserved.
doi:10.1016/j.ijheatmasstransfer.2004.02.010

Nomenclature

A	heating area [m^2]
B, B_0	empirical constants
C, C_0	empirical constants
c_p	coolant specific heat
d	wire diameter [m]
f	friction factor
H	height of testing sample [m]
h	heat transfer coefficient [kW/m^2 K]
L	length of testing sample [m]
l	total height of stacked layers [m]
K_f	coolant thermal conductivity [W/(m K)]
n	total number of screen layers
N	number of pores per unit length, $(N = 1/(w + d))$
Nu_H	nusselt number based on channel height
ΔP	pressure drop [Pa]
Q	input heat [W]
q	heat flux [W/m^2]
R_{open}	open area ratio
Re_H	Reynolds number based on channel height
t	screen layer thickness
$T_{f,\text{bulk}}$	bulk mean temperature of coolant at inlet [K]
T_w	temperature of bottom facesheet [K]
U_{m}	mean coolant velocity at inlet [m/s]
W	width of testing sample [m]
w	width of cell opening [m]

Greek symbols

α_{sf}	surface area density [1/m]
ε	porosity
ρ	density of copper made screens [kg/m^3]
$\bar{\rho}$	relative density

quality (low thermal resistance) metal-to-metal bond (brazing or transient liquid phase bonding is usually preferred over adhesive-bonding) [3]. Applications to electronics cooling and airborne multi-layer metal foam heat exchangers have been investigated, revealing promising advances in the rate of heat removal [6].

While commercial metal foams with open cells, which are typical stochastic cellular structures, are good compact heat exchangers and relatively cheap when made by sintering, their load-bearing capability is much inferior to periodic structures having the same weight. This arises because their deformation under mechanical loading is dominated by cell wall bending as opposed to cell wall stretching in most periodic structures [7]. Nonetheless, as cross-flow heat exchangers they can provide a high thermal conductivity path for heat transport, a very high surface area for dissipation into a cooling fluid located in the pores and a contiguous path for forcing the coolant through the structure.

Topologically configured ultra-light metals with periodic microtruss structures (tetrahedral, pyramidal, Kagome etc.) have subsequently been developed (mainly by rapid prototyping or injection molding, followed by casting), which have good thermal, structural and other performance characteristics [3,8]. A topological comparison between different microtruss structures is made in Fig. 1. Their weight efficiency is as good as the best

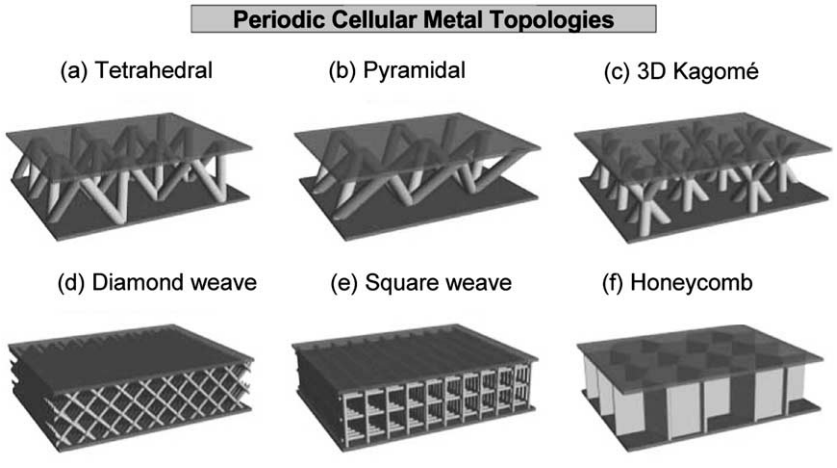

Fig. 1. Topological comparison of periodic structures.

competing concepts, with additional multi-functionality advantages [8], but they are usually costly to manufacture. The use of a metal textile technology coupled with novel bonding strategies to create periodic, cellular structures has the potential to improve the performance/cost ratio [3].

The metal textile derived cellular metals are the three-dimensional analogue of metallic textile screen meshes which have already been extensively used in fields such as aerospace, chemical product, food processing, air conditioning/refrigeration, and medicine [8]. Analytical models, backed with experimental measurements, have been developed to characterize the porosity, flow resistance, and heat transfer of wire-screen meshes [9–15]. Due to anisotropy, the thermal characteristics are orientation dependent, which cause different overall heat transfer in different directions, and hence lead to optimization opportunities. To meet the need for the design of heat pipes and Stirling engine regenerators, a number of studies have focused on predicting the effective thermal conductivity of fluid-saturated wire screens [10,11]. Duprat and Lopez [14] compared the thermal performance of three different heat regenerator media: monolith, stack of woven screens and a packed bed of spheres. Based on a given heat transfer efficiency, the energy efficiency of stacked wire screens was found to cover a wider range of gauges. Ahmad et al. [15] studied the thermo-physical characteristics of various heat transfer media, and found that copper woven screens are promising thermal energy absorber matrices for packed-bed solar air heaters. Hsu et al. [16] developed an analytical model for the effective stagnant thermal conductivity of wire screens.

As far as heat transfer in woven-screen meshes is concerned, previous studies have mainly focused on a single screen layer or self-supporting layers of screens stacked together without bonding. Jiang et al. [17] carried out a combined experimental and numerical study on forced convective heat transfer in packed beds of sintered and non-sintered copper spheres, and found that, due to reduced thermal contact resistance, sintering can increase the overall heat transfer to a cross-flowing fluid. The increases can be large: up to 15 times for water and 30 times for air. We note that such bonding also dramatically modifies the mechanical properties and creates opportunities for multi-functional applications of the type recently envisioned [1,7]. In this study, sandwich panels with woven-screen cores having diamond or square-shaped pores are fabricated by using the TLP bonding and brazing methods to create robust nodes at wire crossovers and between the laminae. The overall heat transfer performance of the panels under forced air convection is measured along different orientations, and is compared with metal foams, microtruss materials, packed beds, louvered fins and other heat dissipation media is made.

2. Test samples

2.1. Fabrication of TLP bonded and brazed textile heat sink

The potentially inexpensive textile-based approach for the synthesis of wire-screen laminates is illustrated in Fig. 2. Prototype sandwich heat sinks with laminated textile cores of plain woven copper cloth (obtained from GDC/City Wire Cloth Co., Fontana, CA) were fabricated using two similar methods: transient liquid phase (TLP) bonding and brazing. The wire alloy was C110000 copper (99.95Cu–0.04O) with a density of $\rho_s = 8.89$ g/cm^3 and a thermal conductivity of $k_s \approx 385$ W/(mK) at ambient conditions.

For TLP bonding operation, laminae were first lightly sprayed with a mix of polymer-based cement (Nicrobraz® Cement 520) and Ni–25Cr–10P braze alloy powder (Nicrobraz® 51), both supplied by Wal Colmonoy Corp. (Madison Heights, MI). The solidus and liquidus of this alloy are 880 and 950 °C whereas the melting point of copper is 1083 °C. The coated laminae were then heated within flowing argon (at a vacuum level of approximately 10^{-1} Torr), at a rate of 20 °C/min to 550 °C to volatilize the polymer cement. An important feature of this braze/cement combination is that the braze alloy powders adhered to the wires after volatilization. The system was then evacuated to a vacuum level of less than 10^{-3} Torr and the temperature was ramped at a rate of 20 °C/min to 1000 °C and held there for 15 min. During this final heating, the braze alloy powders melted, coated the wires (this seals microscopic defects, if any), and the melt was preferentially drawn by capillary action to points of wire contact. This initial node rigidization procedure helps with more accurate stacking and alignment of multiple plies upon laminating. The rigidized laminae were again sprayed with the cement/powder mix and then stacked peak to peak (using pins to align all openings). A small compressive pressure was applied to the periphery of the lay ups and the volatilization/heating procedure was repeated to construct the multi-laminate cores (Fig. 2a). To construct a sandwich, 0.813 mm thick facesheets were sprayed and the volatilization/heating procedure was applied to metallurgically bond them to the textile cores (Fig. 2b). The solid facesheets are made of the same alloy as the wires.

For the brazing operation, individual laminae were stacked, with alignment achieved using threaded guide pins to align all openings. The laminae were stacked peak to peak to ensure a regular structure. A small compressive pressure was then applied to the guide pins to maintain contact at the peak to peak nodes. The entire assembly was then dipped into a viscous brazing paste of CuproBraz®. The CuproBraz® process is a brazing process specifically developed for the manufacturing of automotive and heavy-duty industrial heat exchangers.

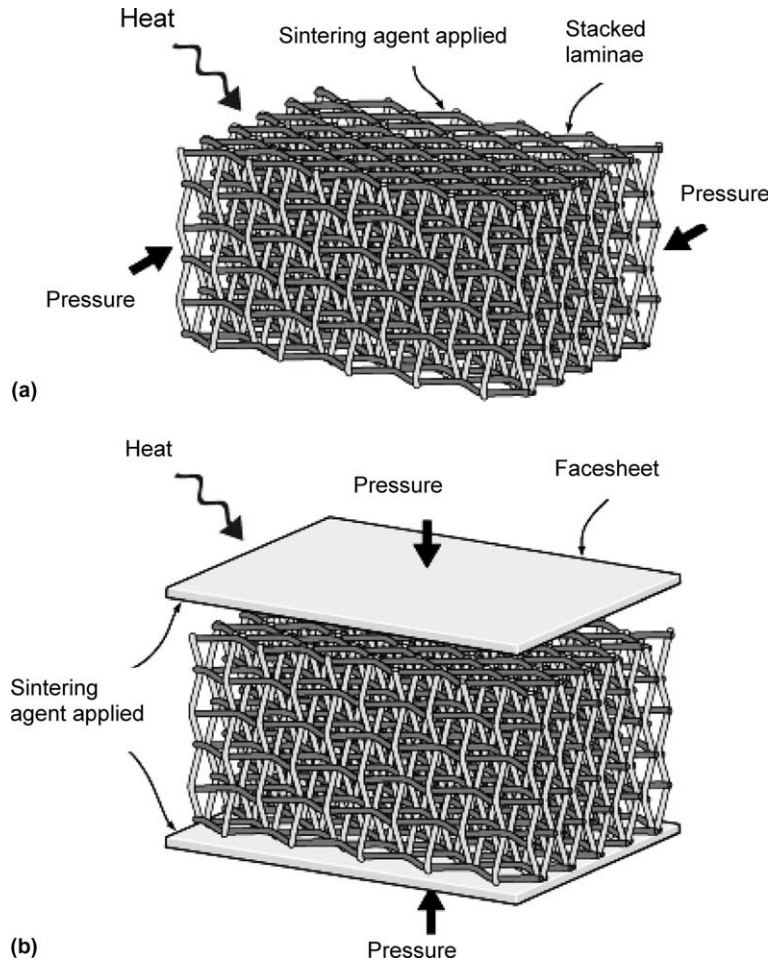

Fig. 2. Sandwich construction with textile technology: (a) a transient liquid phase joins the wire-mesh screen laminated at all points of contact; (b) facesheets are added to the textile core.

By using high strength and high conductivity copper and copper alloys it is possible to manufacture light, strong, efficient and compact heat exchangers at a low cost with this environmentally friendly process. The brazing filler metal, developed for CuproBraz®, belongs to the CuSnNiP-family. This filler metal is called OKC600 and has a nominal composition of: Ni-42%, Sn-15.6%, P-5.3%, Cu-balance. The braze coated assemblies were air dried in a warming oven then transferred to a vacuum furnace and heated under a partial pressure of argon (250 mTorr) at a rate of 30 °C/min to 650 °C and held for 15 min, followed by a rapid furnace cool. Finally, the brazed core assemblies were machined to size and solid copper facesheets were attached using the same brazing process.

The sandwich panels thus created can be designed to carry structural load at minimum weight, while simultaneously allowing fluid passage for cooling or other purposes.

2.2. Topology of textile core

Fig. 3 shows the typical topology of the samples tested; the detail of each test sample is listed in Table 1, where samples made with square-shaped screens are designated S and those with diamond-shaped screens as D. When viewed perpendicular to the mesh, the structure had square or diamond openings with a relative large open area for fluid passage. When viewed from the side, the individual layers formed a triangular pattern with significantly less open fluid passage. The sample sides were machined mutually orthogonal. Samples S-1 and S-2 have identical cores, except for their orientation relative to the facesheet. For sample S-1, the trusses are all parallel to the facesheets, such that the passage of fluid flow is through the stagger-shaped pores between stacked laminate (see Fig. 3a). For samples S-2 to S-4, the trusses are parallel and perpendicular to the facesheets, with flow directed along the aligned square pores (see Fig. 3b).

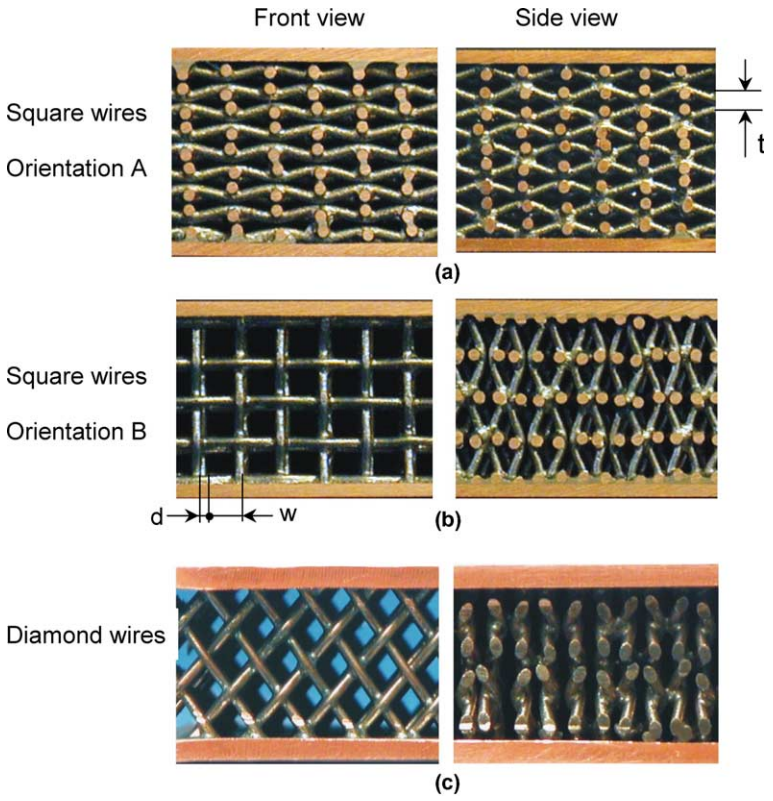

Fig. 3. Textile laminate heat exchangers: (a) images of orientation A with square-shaped pores; (b) images of orientation B with square-shaped pores; (c) images of diamond-shaped pores.

Table 1
Morphological parameters for all brazed wire-screen samples

Sample number	Material make	Wire diameter (mm)	Aperture (mm)	Porosity	Surface area density (m^2/m^3)
Square shape					
Orientation A					
S-1	Pure copper	0.635	1.905	0.798	1237
Orientation B					
S-2		0.635	1.905	0.798	1237
S-3		0.8	1.300	0.680	1496
S-4		0.9	2.800	0.803	849
Diamond shape					
D-1	Pure copper	0.8	2.360	0.795	994
D-2		1.0	2.130	0.737	1004
D-3		1.2	1.980	0.683	988
D-4		0.8	1.300	0.680	1496

For samples D-1 to D-4, the trussed are oriented 45 degree to the facesheets, with flow directed along the aligned diamond pores (see Fig. 3c). All samples have width $W = 40$ mm (same as the width of the testing channel), core height $H = 10$ mm, facesheet thickness 0.813 mm, and length $L = 60$ mm.

2.3. Porosity and surface area density

The woven screens have a wire diameter d, width of square pore w, and screen layer thickness $t = 2d$ (Fig. 3). The number of pores per unit length, N (mesh number), is

$$N = \frac{1}{d + w} \tag{1}$$

For the present samples, N takes the value of 8, 10 and 12 pores/in. With ρ denoting the density of the screens, the relative density of a brazed mesh screen laminate can be calculated as [10]

$$\bar{\rho} \equiv \frac{\rho}{\rho_s} = \frac{\pi N d^2}{2(l/n)} \sqrt{1 + \left(\frac{1}{1 + w/d}\right)^2} \tag{2}$$

where ρ_s is the solid material density, n is the total number of stacked layers of height l, and the effect of bonding has been neglected. As an individual layer is in a bed which can be either compacted or distended, its volume is determined by l/n instead of the wire diameter t. The square-root term in (2) is introduced to account for the effect of crimping of wires during weaving. It has a value less than 1.03 when $w/d > 3$. The measured value of $\bar{\rho}$ is slightly smaller (around 1%) than the value predicted by (2), due to the added weight of bonding agent at contact points.

The porosity ε of the laminate core is related to $\bar{\rho}$ by

$$\varepsilon = 1 - \bar{\rho} \tag{3}$$

Another mesh parameter important for subsequent heat transfer analysis is the surface area density α_{sf} (total surface area per unit volume), given by

$$\alpha_{sf} = \frac{\text{total surface area}}{\text{volume}} = \frac{\pi}{w + d} = \pi N \tag{4}$$

A large surface area density is desirable for enhanced thermal transport in a compact heat exchanger. The surface area density is governed by the number of pores per unit length, N. From Eqs. (2) and (4), α_{sf} increases as the relative density is increased for a given wire diameter. With the relative density fixed, α_{sf} decreases as the wire diameter is increased. The value of α_{sf} can be engineered to exceed 2000 m^2/m^3 when $N > 18$ pores/in. This is comparable to the corresponding value of commercially available metal foams having similar pore sizes. It is significant larger than that of pin fin arrays and microtruss materials having the same relative density, making wire screens potentially attractive as compact heat exchangers.

3. Experiments

3.1. Test set-up and data acquisition procedures

A schematic diagram of the test rig for pressure drop and heat transfer measurements is shown in Fig. 4a. The main components are: air supply, test section, heating arrangement, and data acquisition. An open-circuit suction-type wind tunnel was constructed for this study. Ambient air, as coolant, is drawn into a rectangular Perspex channel (0.025 m width and 0.01 m height) containing the test section. Before reaching the test section, efforts were made to ensure the coolant flow was fully developed. To achieve this, the coolant first flows through a wire-screen layer (wire diameter = 0.56 mm), followed by a 4:1 contraction section, a honeycomb layer, another wire-screen layer, and a relatively long parallel plate channel (with a ratio of section length to channel height, $L1/H = 35$).

A stagnation pressure tapping was placed at the centre and adjacent wall static pressure tapping was used for mid-height flow velocity measurement. Given that the ratio of channel height (10 mm) to outer diameter (0.51 mm) of the tube is 19.6, the wall interference on the pressure tappings is expected to be negligible. The inlet coolant velocity profile along the channel height was measured to calculate the mean flow velocity. For pressure drop measurements, two static pressure tappings monitored by a digital manometer were positioned at the inlet and outlet of the test section, respectively.

Fig. 4b shows the typical inlet coolant velocity profile over the channel height. When the velocity at the mid-height U_c is smaller than 2.7 m/s, the flow is developing; the flow is fully developed when U_c exceeds this value. The mean velocity U_m is correlated with U_c as

$$U_m = 0.84U_c - 0.26 \tag{5}$$

For heat transfer measurement, an isoflux (constant wall heat flux) boundary condition was imposed on the bottom facesheet of the test sandwich by a heating pad (silicone-rubber etched foil from Watlow™ Inc.), whilst the top facesheet is thermally insulated. A pure copper heat spreader plate, 0.9 mm thick, was inserted between the heating element and the bottom facesheet to ensure the uniformity of the heat flux. Four thin (0.013 mm thickness) T-type copper-constantan foil thermocouples (butt bonded) were mounted onto the bottom facesheet along the centreline in the flow direction. Two additional T-type bead thermocouples were positioned separately at the inlet and outlet of the test section to measure the coolant temperature at mid-height at each location. All measurements were performed under steady-state conditions and repeated until significant data repetition was ensured, i.e., 5% uncertainty interval (see measurement uncertainties discussed below). The test conditions are listed in Table 1.

3.2. Data reduction parameters

Experimentally, Kim et al. [18] observed that in an open-celled metal foam with stochastic but otherwise homogeneous cellular structure, fluid-flow pattern repeats over blocks of foam cells (excluding those near the entrance and exit regions). Information obtained from a

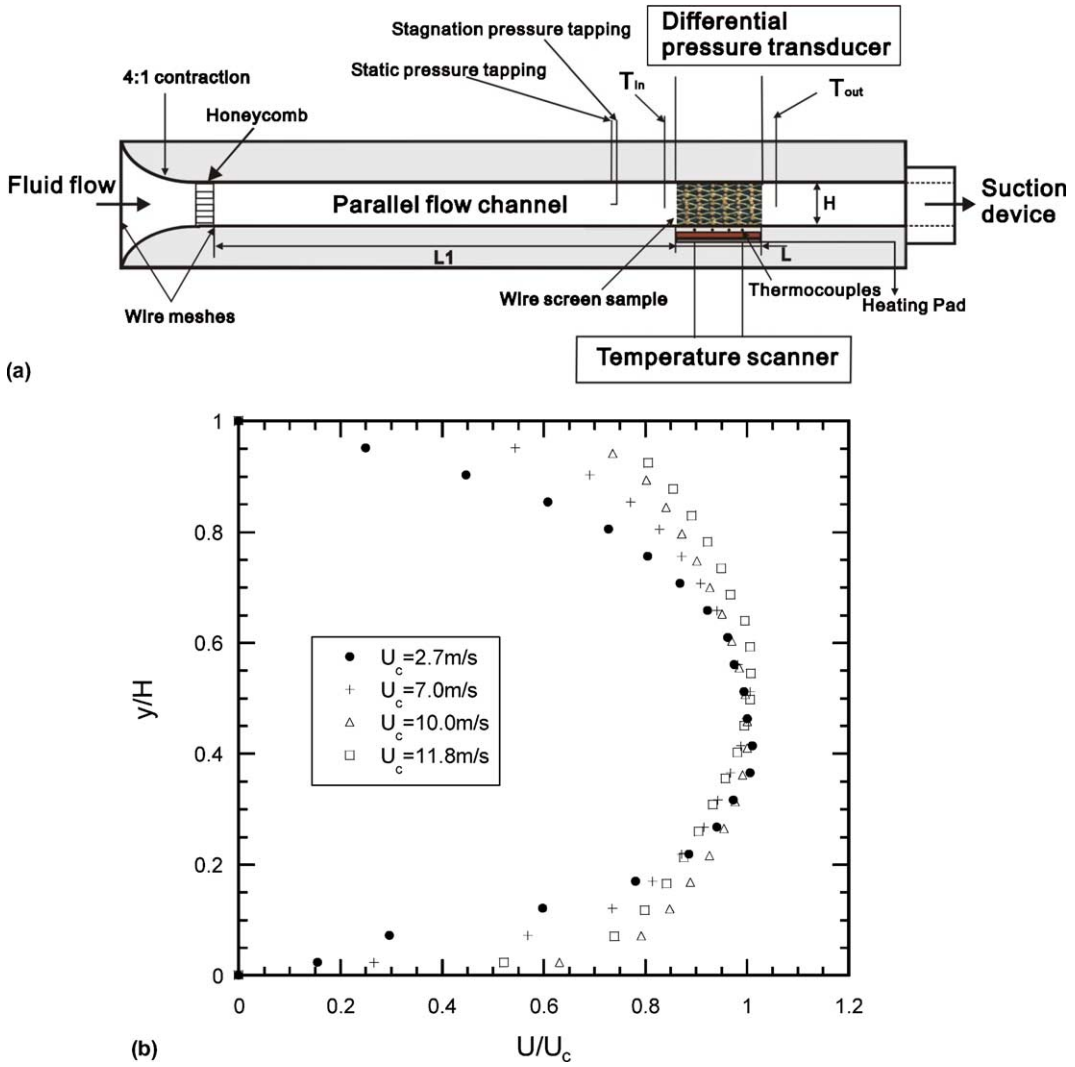

Fig. 4. Experimental set-up: (a) forced air convection test rig; (b) measured inlet flow velocity profile along the channel height.

representative unit cell can therefore be utilized to describe the whole structure. The pressure loss coefficient and Nusselt number defined on the basis of a unit cell have been successfully used by Kim et al. [18] to correlate a multitude of test data from metal foams with different morphological features (pore size, porosity, etc.). In this paper, we use channel height H as the length scale, in order to compare the test data obtained for wire screens with those of traditional heat dissipation media.

Reynolds number and friction factor based on the channel height are defined as

$$Re_H = \frac{\rho_f U_m H}{\mu_f} \tag{6}$$

$$f = \left(\frac{\Delta P}{L}\cdot H\right)\cdot\left(\frac{1}{\rho U_m^2/2}\right) \tag{7}$$

where U_m is the mean coolant velocity at the inlet of the test section, ρ_f and μ_f are the coolant density and viscosity, and $\Delta P/L$ is the pressure drop per unit length. For all the samples tested, the mean inlet coolant velocity varies from 1.0 to 10 m/s (see Fig. 4b). The lower bound of coolant velocity was set by the stability of flow whilst the upper bound was limited by pumping capacity.

For heat transfer characterization, the heat transfer coefficient h and the corresponding Nusselt number Nu_H are defined as

$$h = \frac{Q}{A}\frac{1}{\Delta T} = \frac{q}{T_w - T_{f,\text{bulk}}} \tag{8}$$

$$Nu_H = \frac{h\cdot H}{k_f} \tag{9}$$

where the coordinate x measures from the entrance of the testing sample in the main flow direction, k_f is the thermal conductivity of the coolant, and $q = Q/A$ is the input heat flux. Here, Q is the input rate of heat, A is the heating area (namely, the copper substrate area), T_w is the temperature of the bottom facesheet, and $T_{f,\text{bulk}}$ is the bulk mean temperature of the coolant at inlet.

3.3. Measurement uncertainty

An uncertainty analysis was performed by using the method described in Coleman and Steele [19]. The maximum heat loss through insulation materials was estimated to be less than 2% of the total input heat. The variation in the thermal conductivity of air, k_f, is negligible in the operating temperature range of 300–330 K, whereas its density varies by about 5%. The uncertainty in pressure drop measurement was estimated to be less than 5%. The uncertainties calculated from the root-square method for the mean heat transfer coefficient, Reynolds number and Nusselt number were estimated to be less than 5.3%, 5.7% and 5.4%, respectively.

4. Pressure loss

Ideally, a compact heat exchanger should have a high rate of heat transfer with a low pressure drop. The brazed wire screens are structurally periodic and deterministic but orthotropic. Friction factors of all the test samples are plotted in Fig. 5. Samples tested in different orientations, with different pore shapes and different porosities, show different ranges of friction factors. The relevant parameters of all the samples are summarized in Table 2.

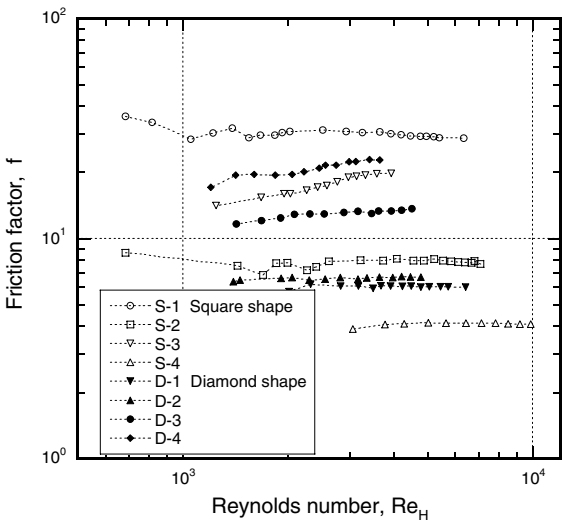

Fig. 5. Friction factor plotted as a function of Reynolds number based on channel height for brazed textiles.

Table 2
Experimental operating conditions

Parameters	Ranges
Inlet coolant velocity	1.0–10 m/s
Reynolds number Re_H	700–10000
Inlet temperature	290.0 K
Outlet temperature	300.0–320.0 K

4.1. Effect of flow orientation

As described in Section 2.2 and seen in Fig. 3, orientation A of a sample has completely different flow passages in comparison with orientation B. The flow passages in the former are staggered, whilst in the latter the flow passages are more open and the pores are square (or diamond) shaped. Therefore, it would be interesting to compare the thermal and hydraulic of samples S-1 and S-2 having identical wire diameter (0.635 mm), pore shape (square), aperture (1.905 mm) and porosity ($\varepsilon = 0.795$), but different orientations.

When $Re_H < 1000$ for S-1 or $Re_H < 1500$ for S-2, the flow is dominated by viscosity (Fig. 5), with the friction factor decreasing with increasing Re_H. At higher Reynolds numbers, the friction factor is nearly constant, as the flow is form dominated. At a given Reynolds number in the form-dominant regime, it is seen from Fig. 5 that the friction factor of S-1 (orientation A) is about three times larger than that of S-2 (orientation B), implying that the resistance encountered by the flow in orientation A is much higher than that in orientation B. For isotropic stochastic materials such as foams and packed beds, friction factor in the high Reynolds number regime is mainly a function of porosity.

Because wire screens are intrinsically anisotropic, flow passages are different along different orientations, even though the porosity remains unchanged. Therefore, parameters in addition to the porosity must be introduced. In order to quantify the contribution of blockage effect on pressure drop, the open area ratio of a sample is defined as

$$R_{\text{open}} = \frac{\text{Open area}}{\text{Total area}} \tag{10}$$

where open area is the void area in the front view, and total area is the whole area in the front view. The open area ratio (0.25) of sample S-1 is approximately half that of sample S-2 (0.56). Consequently, the measured pressure drop across S-2 is significantly lower than that across S-1, implying that the pressure loss in the current range of fluid flow is mainly attributable to the difference in form drag across the wire screens. In general, friction factor increases as the open area ratio is decreased.

4.2. Effect of pore shape

Samples S-3 and D-4 have identical wire diameter, aperture and porosity, but different pore shapes (square versus diamond, see Fig. 3b and c). The friction factor of D-4 is slightly higher than that of S-3, attributable mainly to the cells near top and bottom substrates of the sandwich. Due to machining, these cells are only half or even smaller of a whole unit cell, and hence have different flow patterns in comparison with those in the core centre. However, at high Reynolds numbers, the flow drag behind each wire ligament is the main reason for the overall pressure loss through a wire-screen structure: the contribution caused by the boundary layer near the top and bottom substrates is relatively small.

4.3. Effect of porosity and open area ratio

Fig. 6a and b plot separately the friction factor f as a function of open area ratio R_{open} and porosity ε at $Re_H = 4000$. Note that the flow resistance decreases with increasing R_{open} and increasing ε. Except for sample S-1 (orientation A), Fig. 6a and b exhibit similar trends, suggesting that square shape and diamond shape samples have similar flow patterns. When the flow channel width is much larger than the channel height, the flow resistance mainly depends on flow mixing, with negligible contribution from the partial cells near the substrate walls. Because the open area ratio and porosity are both functions of the ratio of wire diameter to aperture, d/w, porosity can be expressed in terms of open area ratio

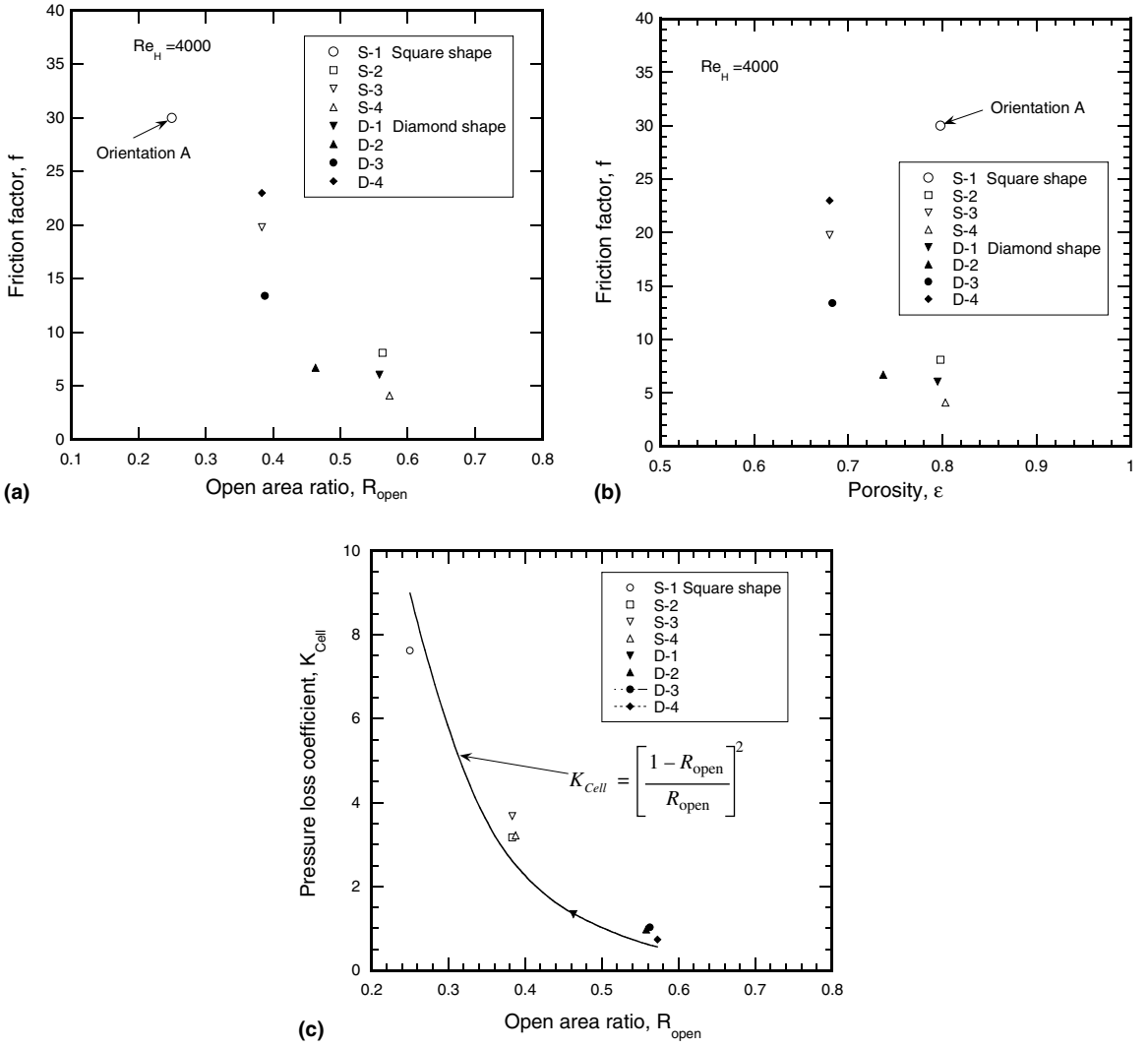

Fig. 6. Effect of (a) porosity and (b) open area ratio on friction factor of woven textiles at $Re_H = 4000$; (c) pressure loss coefficient k_{cell} plotted as a function of open area ratio at $Re_H = 4000$.

and vice versa. However, the results of Fig. 6a and b suggest that R_{open} or ε, both non-dimensional, cannot be used to uniquely characterize the flow resistance of a wire-screen structure: other parameters need to be introduced.

Due to geometrical similarity, the principle of flow passing through an orifice plate may be used to describe pressure loss across a wire screen. The basic mathematical derivations using continuity and momentum equations are given in the Appendix A, leading to a new definition of friction factor (pressure loss coefficient) K_{Cell} based on unit cell length d_p as

$$K_{Cell} = \frac{\Delta P_{Cell}}{\rho U_m^2/2} = \left(\frac{\Delta P}{L}\cdot d_p\right)\cdot\left(\frac{1}{\rho U_m^2/2}\right) = \left(\frac{1-R_{open}}{R_{open}}\right)^2 \quad (11)$$

where, for orientation A, $d_p = d + w$, and for orientation B, $d_p = 2d$. The comparison between the master curve predicted from (11) and experimental data is shown in Fig. 6c for all the samples tested, with reasonably good agreement observed. In other words, the pressure loss across a unit cell can be described by a single parameter R_{open} (or ε). The same conclusion has been reached for stochastic metal foams [18].

5. Heat transfer performance

The heat transfer performance of all the copper structures is compared in Fig. 7, where both the Nusselt number and Reynolds number are based on the channel height. Note that the porosity of wire screens tested in this study ranges from 0.68 to 0.8, significantly smaller than that of metal foam (>0.9) [1,6] but much larger than that of packed beds [2]. Conduction through solid ligaments is therefore more important in brazed wire screens than that in metal foams (as well as that in packed beds without brazing), especially with high thermal conductivity materials (pure copper in current study). The overall heat transfer includes forced convection through wire screens, conduction through substrates as well as wire screens.

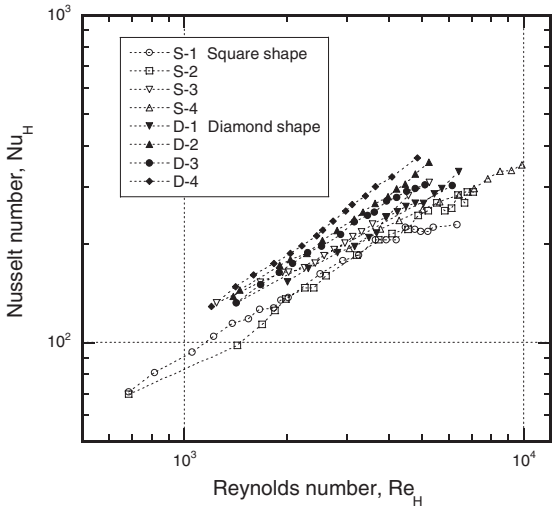

Fig. 7. Nusselt number plotted as a function of Reynolds number based on channel height for woven textiles.

5.1. Effect of flow orientation

At a given Reynolds number, Sample S-2 has a larger Nusselt number than that of S-1 (Fig. 7), even though its flow resistance is much smaller than the latter (Fig. 5). Also, the heat transfer rate of S-2 increases slightly faster than S-1 as the Reynolds number is increased (Fig. 7).

As can be seen from Fig. 3, S-2 has a continuous solid path along the channel height, whilst S-1 has brazed joints between stacked layers. The material between joints is nickel, with a thermal conductivity much smaller than pure copper. It is expected therefore that S-2 has a larger effective thermal conductivity along the channel height than that of S-1. This is important because, during the experiment, heat is supplied from the bottom facesheet while fluid flows in a direction perpendicular to the direction of heat.

Another likely reason for the superior performance of S-2 to S-1 lies in the different flow patterns in these two samples. From the well established study of bank of cylinders, it is known that the flow pattern behind one cylinder depends on the arrangement of cylinders. If the distance of two rows of cylinder is too close, the vortex after the first row is yet to complete when the new vortex starts; on the other hand, if the distance is sufficiently large for vortexes to complete, the flow is less turbulent. From the heat transfer point of view, the flow pattern developed in S-1 is not as efficient as that in S-2, even though the flow encounters much higher resistance in S-1.

5.2. Effect of pore shape

Samples S-3 and D-4 are identical, except that the pores in the former are square and those in the latter are diamond. Because both samples have approximately the same flow resistance (Fig. 5) and flow pattern (excluding regions near the substrates), it is expected that the contribution of forced convection on the overall heat transfer is nearly the same for these two samples. However, the experimental data in Fig. 7 reveal that the Nusselt number of D-4 is 20–30% higher than that of S-3. The difference is mainly attributable to the different contribution from conduction through wire ligaments. From Fig. 3, it can be seen that the solid wire elements in

a diamond shape sample (D-4) have approximately 40% more contact area with the substrates than those in a square shape sample (S-3), leading to a higher effective thermal conductivity in the direction of channel height. If the two samples are made with a low conductivity material (e.g., polymer), they would have the same heat dissipation capability because the contribution from solid conduction is negligible in comparison with that due to convection. This has been verified experimentally by Kim et al. [20] for lattice-frame materials.

5.3. Effect of porosity and surface area density

Surface area density represents the total surface area per unit volume, whereas porosity represents the percentage of void per unit volume. Because pure copper has a high thermal conductivity, the contribution of thermal conduction through wire ligaments cannot be ignored. Consequently, both the surface area density and porosity are important characteristics for copper wire meshes. In the following discussion, one of the two parameters is fixed while the other is varied in order to isolate the effects.

Fig. 8a plots the Nusselt number of samples D-1, D-2 and D-3 as a function of porosity; the surface area density of the three samples with diamond-shaped pores is approximately 1000 m^{-1} and Reynolds number is fixed at 4000. The overall heat transfer rate appears to decrease if the porosity is increased beyond 0.75 or decreased below 0.70. Higher porosity means less solid material per unit volume, and hence less conduction through wire ligaments. Lower porosity means less void volume per unit volume, and hence less contribution of forced convection. It is likely therefore that there exists an optimal porosity for maximum heat transfer at a given surface area density. For the samples tested here, this porosity lies in the range between 0.7 and 0.75. More experiments, complemented with theoretical modelling, will be conducted in a future study to further highlight this important feature of cellular structures made with a high conductivity material.

Fig. 8b illustrates the effect of surface area density on the heat transfer capability of samples D-2, D-3 and D-4 at a fixed porosity level ($\varepsilon \cong 0.7$) and a given Reynolds number ($Re_H = 4000$). At a given porosity, the amount of heat dissipated increases with increasing surface area density. A higher surface area density corresponds to a larger surface area per unit volume between fluid and solid, and hence more heat can be transferred by the fluid.

6. Comparison of heat dissipation media

The following different types of porous heat dissipation medium listed in Table 3 are compared: brazed copper textiles (excluding S-1 with orientation A), lattice-frame materials (LFMs, aluminum alloy) [20,21], Kagome structures (bronze) [22], metal foams (copper and FeCrAlY—a steel alloy) fabricated with the relatively cheap sintering route [23,24], aluminum foams made with the expensive investment casting route [25], packed beds with non-sintered steel beads and with sintered bronze beads [26], aluminum louver fin arrays [27], and corrugated ducts with sinusoidal wavy passages [28]; empty channel [29] is also included as datum.

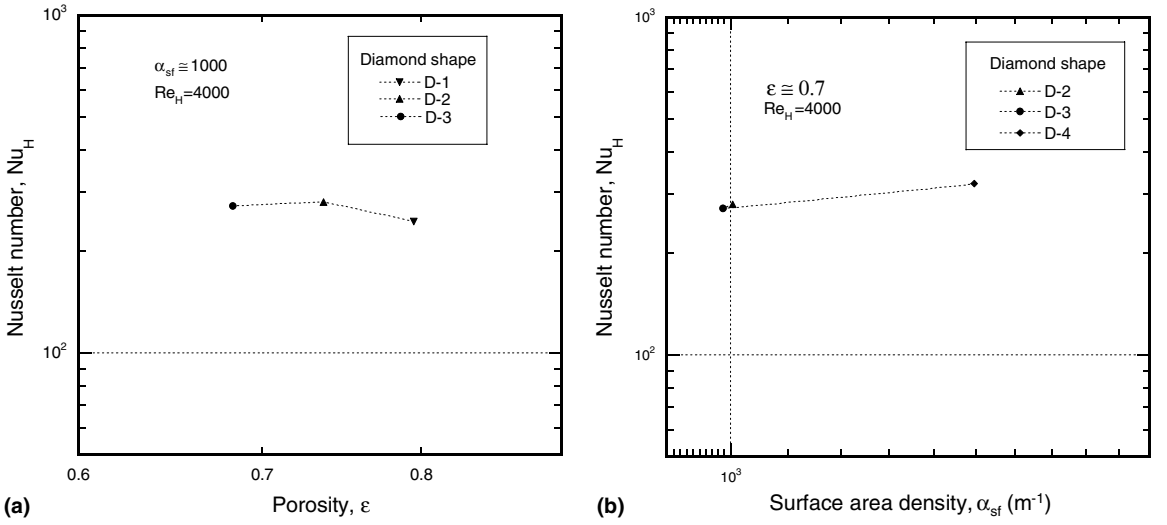

Fig. 8. Effect of (a) porosity with fixed surface area density and (b) surface area density with fixed porosity on Nusselt number at $Re_H = 4000$.

Table 3
Data for all materials used in performance comparison

Material	H [mm]	Porosity	Pore size [mm]	U [m/s]	h [W/m^2 K]	Re_H	f	Nu_H	Nu/f	$Nu/f^{1/3}$
Brazed copper wire screens	10	0.69–0.80		0.93–7.8	170–703	685–7000	5–15	70.6–500	8–37.4	35.3–144
Sintered FeCrAlY foams	12	0.822–0.917	1.0–3.0	2.2–14.2	130–477	2000–11 000	4–80	57–217	1–28	22–120
Sintered copper foams	12	0.881–0.94	0.55–3.0	0.67–10	77–728	550–8200	13–88	35–332	0.4–20	20–141
Lattice-frame materials (aluminum alloy LM25)	12	0.938	12.7–14.7	1.84–21.4	125–482	1500–18 000	0.61	57–220	93–360	67–259
LFMs (polycarbonate)								30–110	47–180	35–129
Kagomé (BeCu)	12	0.926–0.971	12.2–14.7	1.54–31.5	109–563	1200–27 000	0.3–0.64	50–257	120–700	58–383
Kagomé (polycarbonate)								25–154	70–420	29–230
Aluminum foams	9	0.92	1.6–3.9	1.1–5.4	115–400	570–2800	6.1–13.5	39–140	4.8–15	16–77
Packed beds (sintered bronze beads)	10.87	0.444	1.0–1.4	$f = 307506/Re_H + 217.5$ $Nu_H = 0.0634 Re_H^{1.0566}$		500–20 000	221–833	45–12164	0.06–55	5–2013
Packed beds (non-sintered steel beads)	10	0.4	1.2	$f = 94938/Re_H + 155.4$ $Nu_H = 1.2503 Re_H^{0.4732}$		500–20 000	156–345	24–291	0.07–1.9	3.4–54
Aluminum louvered fins	4.45			2–33	47.5–316	600–10 000	0.06–0.4	8–53.5	80–1115	17–147
Corrugated ducts						250–2000	0.22–0.4	9–30	22.5–136	12–50
Empty channel	Laminar regime		$f = 64/Re$, $Nu \sim$ constant			100–2000	0.02–0.64	8.3	12–386	9–30
	Turbulent regime		$Nu = 0.023(Re)^{0.8} Pr^{0.4}$			2500–30 000	0.02–0.04	12–78.1	203–3900	35–228

LFMs and Kagome structures are both periodic and highly porous ($\varepsilon \sim 0.9$), consisting a 3D network of cylindrical trusses. The porosity of the packed beds is low, about 0.4.

The design of a good heat exchanger demands a high heat transfer rate and a low mechanical pumping power needed to overcome fluid friction (pressure drop) and move the fluid(s) through the heat exchanger. Hence, three aspects have been considered below: pressure drop, heat transfer rate, and the ratio of heat transfer rate to pressure drop, with the channel height selected as the characteristic length scale for each medium [24].

6.1. Pressure loss

The comparison of overall pressure loss for different heat dissipation media is shown in Fig. 9a for a wide range of Reynolds numbers. Flow past packed beds experiences the highest drag. The typical flow resistance of foam materials is about two orders of magnitude larger than that of the empty channel. It is also much larger than that of periodic materials such as textiles, Kagome structures and LFMs, even though the porosity of foams is high (comparable with Kagome structures and LFM but significantly larger than textiles), highlighting the main difference between stochastic and

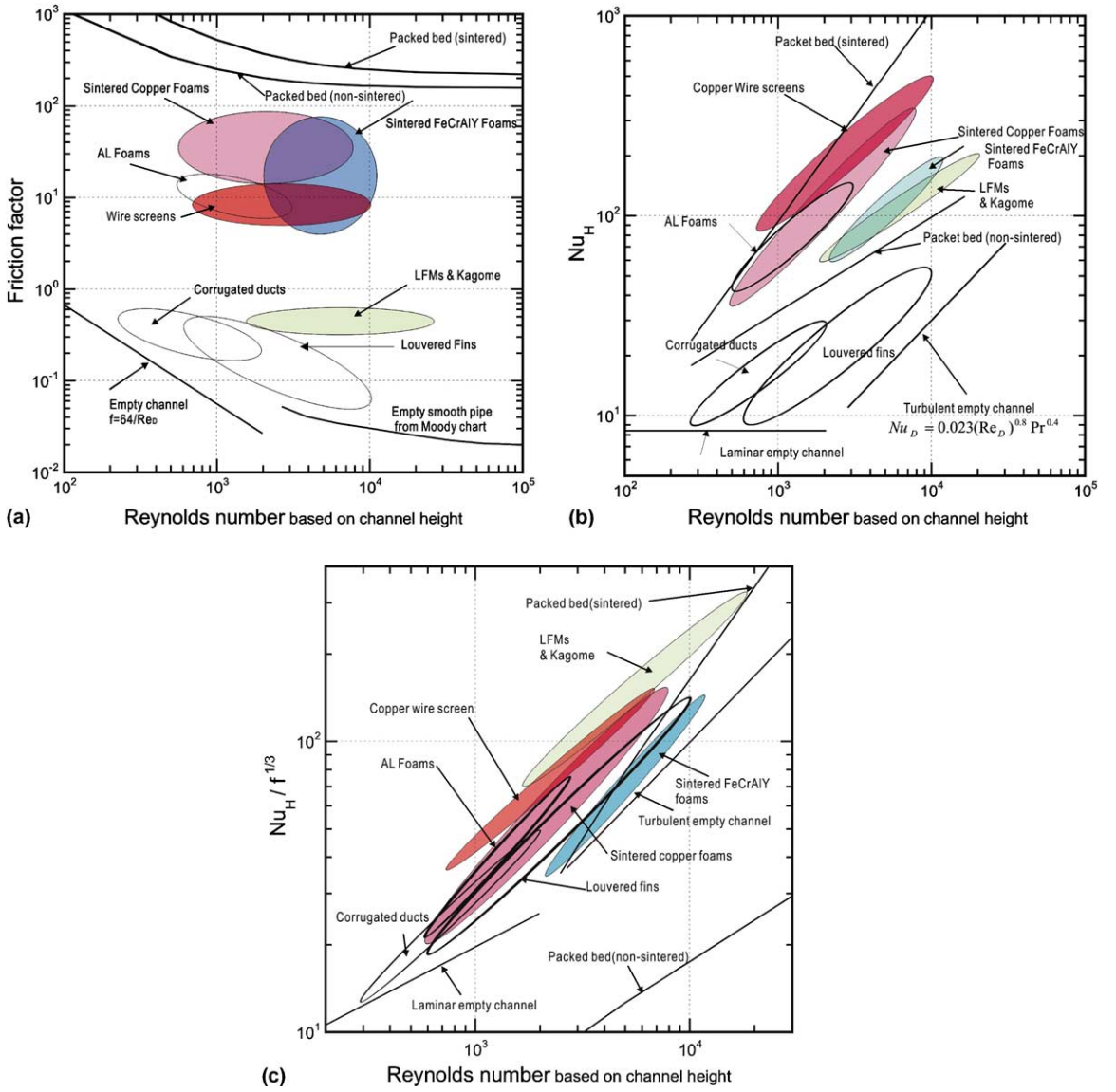

Fig. 9. Performance charts of different heat dissipation media: (a) friction factor; (b) heat transfer; (c) efficiency index $Nu_H/f^{1/3}$.

periodic materials due to the difference in flow patterns. The flow resistance of LFMs and Kagome structures is about 10 times higher than that of an empty channel, but lower than that of wire screens. Both materials are periodic but have different porosities, with $\varepsilon = 0.7$–08 for wire screens and $\varepsilon \sim 0.9$ for LFMs and Kagome structures. For periodic materials, porosity (as well as pore size) is the main characteristic dictating pressure loss. The selection of flow direction relative to pore topology is also important as discussed in Section 4.

6.2. Heat transfer

Fig. 9b compares the heat transfer performance of different heat dissipation media. Copper wire screens, copper foams, aluminum foams and packed beds with sintered bronze beads outperform corrugated ducts and louvered fins. Heat dissipation in the former group is contributed by both forced convection and conduction through the network of solid ligaments, whereas that in the second group depends mainly on the change in flow patterns caused by augment heat transfer surfaces. The copper wire screens tested in this study have porosities close to the optimal level ($\varepsilon \approx 0.75$) that corresponds to the optimal combination of forced convection and solid conduction. Because of high porosity ($\varepsilon > 0.9$) of foams, the contribution of solid conduction to the overall heat transfer is not as significant as that due to forced convection. This explains why there is no considerable difference in terms of Nusselt number between foams made with high conductivity materials (copper and aluminum) and low conductivity materials (steel alloy). For packed beds, the high thermal contact resistance amongst non-sintered particles causes significantly inferior overall heat transfer performance to that of sintered particles.

6.3. Thermal efficiency

To compare the overall performance of different heat dissipation media, a thermal efficiency index defined using the average Nusselt number Nu_H and the friction factor f based on channel height will be used. Traditionally, this is done using the empirical index Nu_H/f. Whist this index may be useful to rank the performance of a series of heat exchangers having different geometrical parameters but same topological configuration (e.g., different louver fin arrays, or metal foams with different pore sizes and porosities), it is not adequate to compare the performance of different classes of heat exchangers. For example, amongst the heat dissipation media considered in this work, the empty channel and louvered fin arrays have the best overall performance due mainly to the low pressure loss. Although foams have higher heat transfer rate, they have the lowest efficiency index due to high flow resistance as a result of stochastic cellular morphology. In other words, according to this index, metal foams and copper textiles are inferior to an empty channel. Consequently, the adequacy of the above thermal efficiency index is questionable, and a modified efficiency index is used below.

Since the pumping power Q is equal to pressure drop Δp times the volumetric flow rate, dimensional analysis dictates that:

$$Q \sim \Delta P u L^3, \quad f \sim \frac{\Delta P}{u^2}, \quad Re \sim uL \tag{12}$$

and hence

$$Q \sim fRe^3 \tag{13}$$

Consequently, the thermal efficiency index can be introduced as

$$\text{Efficiency index} = Nu_H/f^{1/3} \tag{14}$$

Performance charts plotted using $Nu_H/f^{1/3}$ as one axis and Re_H as another are shown in Fig. 9c for stochastic materials, periodic structures, packed beds, louvered fins, corrugated ducts and empty channel. Physically, these charts rank the heat transfer capabilities of these heat dissipation media at a *fixed* pumping power. Fig. 9c reveals that all the heat dissipation media considered in this paper are better heat exchangers than an empty channel, except for the packed bed with non-sintered metallic particles. Note also that, in the form-dominated regime ($Re_H > 1000$), periodic materials (LFMs, Kagome structures and copper textiles) have superior thermal efficiency to other media, and their overall performance may be further enhanced by optimizing the topology and porosity.

7. Conclusions

The overall pressure drop and heat transfer of brazed copper textile meshes have been experimentally investigated under steady-state forced air convection conditions. Prototype sandwiches with different topological configurations were tested along different flow orientations, with uniform heat flux boundary condition imposed.

For the range of Reynolds numbers considered, fluid flow in all textile meshes is form dominated: the friction factor in all cases is independent of the coolant velocity. The friction factor based on the unit pore size depends mainly on the open area ratio. If channel height is chosen as the length scale, then the friction factor is also a function of pore size and flow direction.

The transfer of heat across the meshes depends on two competing mechanisms: solid conduction and forced convection. At a given Reynolds number, porosity and surface area density are two key parameters controlling heat transfer. At a given porosity, the

heat dissipation rate increases as the surface area density is increased. With increasing porosity, conduction decreases while convection increases. Consequently, for a fixed surface area density, there exists an optimal porosity for maximum heat dissipation. For the copper textiles studied, this optimal porosity is about 0.75.

Performance charts are presented to compare copper textiles with selected heat dissipation media including metal foams, Kagome structures, lattice-frame materials, packed beds, corrugated ducts and louvered fins. Thermally, the copper textiles are as good as the stochastic metal foams, both having large surface area densities. However, the pumping power required is significantly lower for the textiles, because the periodic topology can be selected according to performance expectations: their overall thermal efficiency is about three times larger than that of copper foams. Significant opportunities exist to maximize the heat transfer performance of periodic cellular metals by varying the pore fraction, anisotropy of the pores and metallic alloy used. For multi-functional applications, further optimization requires simultaneous consideration of their thermal and structural properties.

Acknowledgements

The work was supported by the U.S. Office of Naval Research through ONR/ONRIFO grant number N000140110271 and ONR grant number N0001400-10342, and by the U.K. Engineering and Physical Sciences Research Council (EPSRC grant number EJA/U83).

Appendix A. Flow through an orifice plate

Consider the two-dimensional flow through an orifice plate as shown in Fig. 10. The orifice plate is introduced to model one unit cell of the periodic woven textile. Let A_1, A_2 and A_3 denote the cross-sectional area of the flow before (inlet), at and after (outlet) the orifice, and let (u_1, u_2, u_3) and (p_1, p_2, p_3) denote the corresponding flow velocities and pressures. The continuity of mass dictates

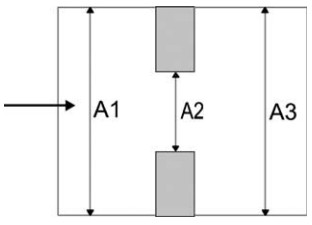

Fig. 10. Flow through an orifice plate.

$$\rho u_1 A_1 = \rho u_2 A_2 = \rho u_3 A_3 \tag{A.1}$$

when $A_1 = A_2$, $u_1 = u_3$. Similarly,

$$\frac{u_2}{u_3} = \frac{A_3}{A_2} \tag{A.2}$$

The momentum equation requires

$$P_2 A_3 + \rho u_2 u_2 A_2 = P_3 A_3 + \rho u_3 u_3 A_3 \tag{A.3}$$

The pressure drop from location 2 to location 3 is

$$P_2 - P_3 = \rho u_3^2 - \rho u_2^2 \frac{A_2}{A_3} \tag{A.4}$$

and the Bernoulli equation is given by

$$P_1 - P_2 = \frac{1}{2}\rho(u_2^2 - u_1^2) \tag{A.5}$$

Combining Eqs. (A.1)–(A.5), one obtains the friction factor based on the unit cell size as

$$K_{\text{Cell}} = \frac{P_1 - P_3}{\rho u_1^2/2} = \left(\frac{1 - R_{\text{open}}}{R_{\text{open}}}\right)^2 \tag{A.6}$$

where $R_{\text{open}} = A_2/A_3$ is the open area ratio of the orifice plate.

References

[1] M.F. Ashby, A.G. Evans, N.F. Fleck, L.J. Gibson, J.W. Hutchinson, H.N.G. Wadley, Metal Foams: A Design Guide, Butterworth-Heineman, 2000.
[2] M. Kaviany, Principles of Heat Transfer in Porous Media, Springer, New York, 1995.
[3] D.J. Sypeck, H.N.G. Wadley, Multifunctional microtruss laminates: textile synthesis and properties, J. Mater. Res. 16 (2001) 890–897.
[4] J. Tian, T. Kim, T.J. Lu, H.P. Hodson, D.J. Sypeck, H.N.G. Wadley, The effects of topology upon fluid-flow and heat-transfer within cellular copper structures, in: Proceedings of 8th UK National Heat Transfer Conference, Oxford, 9–10 September 2003.
[5] H.N.G. Wadley, Cellular metals manufacturing, Adv. Eng. Mater. 4 (2002) 726–733.
[6] T.J. Lu, H.A. Stone, M.F. Ashby, Heat transfer in open-cell metal foams, Acta Mater. 46 (1998) 3619–3635.
[7] A.G. Evans, J.W. Hutchinson, N.A. Fleck, M.F. Ashby, H.N.G. Wadley, The topological design of multifunctional cellular metals, Prog. Mater. Sci. 46 (2001) 309–327.
[8] D.R. Mumm, A.G. Evans, D.J. Sypeck, H.N.G. Wadley, On the performance of light weight metallic panels fabricated using textile technology, Materials Science and Engineering A, submitted.
[9] J.C. Armour, J.N. Cannon, Fluid flow through woven screens, AIChE J. 14 (1968) 415–421.
[10] W.S. Chang, Porosity and effective thermal conductivity of wire screens, ASME J. Heat Transfer 112 (1990) 5–9.

[11] J.R. Sodré, J.A.R. Parise, Friction factor determination for flow through finite wire-mesh woven-screen matrices, ASME J. Fluid Eng. 119 (1997) 847–851.
[12] D. Mehta, M.A. Hawley, Wall effect in packed columns, I&EC Process Des. Dev. 8 (1969) 280–282.
[13] S. Ergun, Fluid flow trough packed columns, Chem. Eng. Prog. 48 (1952) 89–94.
[14] F. Duprat, G. Lopez, Comparison of performance of heat regenerators: relation between heat transfer efficiency and pressure drop, Int. J. Energy Res. 25 (2001) 319–329.
[15] A. Ahmad, J. Saini, H. Varma, Effect of geometrical and thermo-physical characteristics of bed materials on the enhancement of thermal performance of packed-bed solar air heaters, Energy Convers. Manage. 36 (1995) 1185–1195.
[16] C.T. Hsu, K.W. Wong, P. Cheng, Effective stagnant thermal conductivity of wire screen, J. Thermophys. 10 (1996) 542–545.
[17] P. Jiang, M. Li, T.J. Lu, Z. Ren, X. Sun, Convection heat transfer in sintered porous plate channels, in: Proceedings of 12th International Conference on Heat Transfer, Grenoble, France, August 2002.
[18] T. Kim, A.J. Fuller, H.P. Hodson, T.J. Lu, An experimental study on thermal transport in lightweight metal foams at high Reynolds numbers, in: Proceedings of International Symposium of Compact Heat Exchangers, Grenoble, France, 2002, pp. 227–232.
[19] H.W. Coleman, W.G. Steele, Experimentation and Uncertainty Analysis for Engineers, second ed., John Wiley & Sons Inc., 1999.
[20] T. Kim, C.Y. Zhao, T.J. Lu, H.P. Hodson, Convective heat dissipation with lattice-frame materials, Mech. Mater., in press.
[21] T. Kim, Fluid-flow and heat-transfer in a lattice-frame material, PhD Thesis, Department of Engineering, University of Cambridge, 2003.
[22] F. Hoffmann, T.J. Lu, H.P. Hodson, Heat transfer performance of Kagome structures, in: Proceedings of 8th UK National Heat Transfer Conference, Oxford, 9–10 September 2003.
[23] C.Y. Zhao, Thermal transport in cellular metal foams with open cells, PhD Thesis, Department of Engineering, University of Cambridge, 2003.
[24] C.Y. Zhao, T. Kim, T.J. Lu, H.P. Hodson, Thermal transport in high porosity cellular metal foams, J. Thermophys. Heat Transfer, in press.
[25] S.Y. Kim, B.H. Kang, J.H. Kim, Forced convection from aluminum foams in an asymmetrically heated channel, Int. J. Heat Mass Transfer 44 (2001) 1451–1454.
[26] P.X. Jiang, M. Li, T.J. Lu, Z. Ren, X. Sun, Convection heat transfer in sintered porous plate channels, in: Proceedings of 12th International Conference on Heat Transfer, Grenoble, France, August 2002.
[27] W.M. Kays, A.L. London, Compact Heat Exchangers, third ed., McGraw-Hill, Lond, 1984.
[28] H. Blomerius, C. Holsken, N.K. Mitra, Numerical investigation of flow field and heat transfer in cross-corrugated ducts, ASME J. Heat Transfer 121 (1999) 314–321.
[29] F.W. Dittus, L.M.K. Boelter, Heat transfer in automobile radiators of the tubular type, Univ. California Publ. Eng. 2 (1930) 443–461.